Nuclear Inst, and Methods in Physics Research B 430 (2018) 59–63

Contents lists available at ScienceDirect

Nuclear Inst. and Methods in Physics Research B

journal homepage: www.elsevier.com/locate/nimb

Degradation in AlGaN/GaN HEMTs irradiated with swift heavy ions: Role of latent tracks

P.P. Hu[a,b], J. Liu[a,*], S.X. Zhang[a], K. Maaz[c], J. Zeng[a], P.F. Zhai[a], L.J. Xu[a,b], Y.R. Cao[d], J.L. Duan[a], Z.Z. Li[a,b], Y.M. Sun[a], X.H. Ma[e]

[a] Institute of Modern Physics, Chinese Academy of Sciences (CAS), Lanzhou 730000, PR China
[b] University of Chinese Academy of Sciences (UCAS), Beijing 100049, PR China
[c] Nanomaterials Research Group, Physics Division, PINSTECH, Nilore 45650, Islamabad, Pakistan
[d] School of Mechano-Electronic Engineering, Xidian University, Xi'an 710071, PR China
[e] School of Advanced Material and Nanotechnology, Xidian University, Xi'an 710071, PR China

ARTICLE INFO

Keywords:
GaN
HEMT
Swift heavy ion
Latent track
Electrical characteristics

ABSTRACT

AlGaN/GaN high electron mobility transistor (HEMT) devices were irradiated with swift heavy ions at different fluences. From structural and electrical studies, it was found that SHI irradiation leads to a significant deterioration of structural and electrical properties of the devices. Positive threshold voltage V_{th} was found to increase by about 85% as a result of irradiation with 1540-MeV ^{209}Bi ions at fluence of 1.7×10^{11} ions/cm^2, while this threshold voltage value was increased by 55% after irradiation with 2300-MeV ^{129}Xe at a fluence of 4×10^{11} ions/cm^2. The maximum saturation drain current I_{ds} was decreased by about two orders of magnitude in the device after irradiation with ^{209}Bi ions. Quasi-continuous tracks were observed visually in the devices after irradiation with ^{209}Bi ions. The observed defects and disorders induced in the devices by SHI irradiation were found responsible for the decrease in carrier mobility and sheet carrier density, and finally, these defects resulted in the degradation of electrical characteristics of HEMTs.

1. Introduction

Gallium nitride (GaN) is a typical wide bandgap semiconductor material that belongs to III–V group with excellent physical and chemical properties. Materials based on GaN are known to be advantageous for the fabrication of high-power electronic devices including high breakdown voltage diodes, power amplifiers, and power switches [1]. Moreover, GaN-based devices such as high electron mobility transistors (HEMTs) and light emitting diodes are promising in the field of optoelectronics [2–6]. GaN as a third-generation semiconductor can overcome the limitations of traditional Si electronic devices; it can be operated widely at high temperatures, pressures, and radiation and even in more extreme and harsh environments [7–9]. This creates considerable interest in GaN-based materials to understand the mechanisms of various radiation effects and their reliability in the devices. Several phenomena including hot phonon effects [10], inverse piezoelectric effects [11], and hot carrier effects [12] were proposed to study the influence of radiation in GaN-based devices. However, the exact mechanism remains unclear and needs to be investigated in detail.

It is well understood that the properties of the device are strongly associated with the characteristics of GaN-based materials. The reliability of the devices is strongly affected by the defects and stresses in the material that are induced by radiation. As reported by Hazdra et al. [13], the radiation defects created by 4.5-MeV electrons are responsible for the decrease in electron concentration and mobility at much higher doses. In an experiment with 2-MeV proton irradiation, it was indicated that defects that appeared at AlGaN/GaN interface act as the scattering centers near the two-dimensional electron gas (2DEG) that resulted in the reduced mobility of the device [14]. GaN HEMTs exhibit a high radiation resistance to gamma-rays, although at high fluences, the gamma-ray irradiation can also induce additional traps that can significantly influence the electrical and optical characteristics of the devices [15]. Moreover, it was found that after thermal neutron irradiation, the reverse-bias current of GaN PIN diodes was significantly increased due to the irradiation-induced defects in GaN and defects near the metal/GaN interface [16]. To date, the interaction of energetic ions with GaN and GaN-based devices arises mostly due to the low-energy ions, when the nuclear energy loss is considered the primary energy transfer mechanism [17,18]. Thus far, the microstructure damage of GaN-based devices caused by the swift heavy ion (SHI)

* Corresponding author.
E-mail address: j.liu@impcas.ac.cn (J. Liu).

https://doi.org/10.1016/j.nimb.2018.06.011
Received 26 February 2018; Received in revised form 11 June 2018; Accepted 11 June 2018
Available online 18 June 2018
0168-583X/

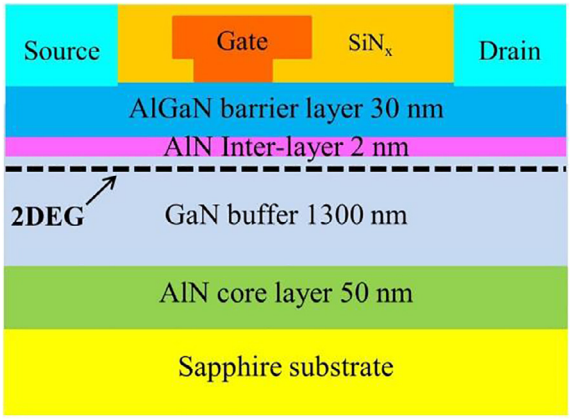

Fig. 1. Heterojunction cross-sectional diagram of AlGaN/GaN HEMT.

irradiation has not been extensively studied. In this work, we carry out a series of SHI irradiation experiments to study the irradiation effects on the structure evolution and electrical properties of GaN-based HEMT devices, to find an essential correlation between the degradation of electronical characteristics and damages that occur in the microstructure of the devices.

2. Experimental method

AlGaN/GaN HEMT devices were fabricated by metal-organic chemical vapor deposition (MOCVD) technique. The heterojunction cross-sectional diagram of AlGaN/GaN HEMT is shown in Fig. 1. The structure consist of a 50-nm AlN core layer on a sapphire substrate, 1.3-μm-thick GaN buffer layer without any dopant, 2-nm AlN insert layer, and 30-nm AlGaN barrier layer with aluminum mole fractions of 25–30%. Standard lift-off procedure was adopted to form the ohmic metal source and drain (Ti/Al/Ni/Au) and the gate metal (Ni/Au) contacts. Finally, all the samples were passivated with SiN_x to eliminate the surface state and increase the surface density of channel carriers [19].

Irradiation experiments were performed at the Heavy Ion Research Facility in Lanzhou (HIRFL) in which the AlGaN/GaN HEMT devices were irradiated with ^{209}Bi and ^{129}Xe ions with initial kinetic energies of 9.5 and 19.5 MeV/u, respectively. The devices were in off-sate without bias during the irradiation process. Ion beam scanning was used to obtain homogeneous irradiation under normal incidence at room temperature in vacuum. The detailed irradiation parameters in GaN material calculated by SRIM-2013 code [20,21] are presented in Table 1. We also calculated the energy loss in the upper layers before the ions were incident on the GaN layer, and it was found that the maximum energy loss was lower than 10 MeV, while the corresponding electronic energy loss of the ions was reduced by less than 0.06%. Therefore, the energy loss of the ions caused by the electrode and the passivation layers can be neglected. The electrical parameters of the pristine and irradiated AlGaN/GaN HEMT devices were measured using a semiconductor parameter analyzer (4200A-SCS), and then a cross-sectional transmission electron microscope (TEM, FEI Tecnai G2 TF-20, 200 kV) was used to investigate the structural damage of the devices. The cross-sectional images of the devices selected for TEM measurement were obtained using a focus ion beam system (FIB, FEI Helio 600).

Table 1
Irradiation parameters in the experiment, $(dE/dx)_e$ and $(dE/dx)_n$ denote the electronic and nuclear energy losses in GaN, respectively, as calculated using SRIM-2013 code [20,21].

Ion	Energy/ (MeV)	$(dE/dx)_e$/ (keV/nm)	$(dE/dx)_n$/ (10^{-2} keV/nm)	Projected range/(μm)	Fluence /(ions/cm^2)
$^{209}Bi^{31+}$	1540	45.9	6.5	40.9	1.7×10^{11}
$^{129}Xe^{27+}$	2300	22.9	1.4	86.7	4×10^{11}

3. Results and discussion

3.1. Transfer characteristics and output characteristics

The pristine and irradiated HEMT devices were tested with a drain-source voltage of 10 V and gate voltage V_{gs} that was increased from −6 V to 2 V. The transfer characteristics showed significant changes after irradiation of the devices. The results for the two devices are shown in Fig. 2. It is seen that, the threshold voltage V_{th} increased from −5.4 V to −0.8 V, thereby showing an increase of 85% in V_{th} value for the devices irradiated with 1540-MeV ^{209}Bi ions, whereas the drain current decreased to 1% of its initial value [Fig. 2(a)]. A similar phenomenon was observed in the devices irradiated with 2300-MeV ^{129}Xe ions at a high fluence. In this case, V_{th} increased from −5.5 V to −2.5 V showing around 55% increase, and the corresponding drain current was decreased by about 60% as compared to the pristine HEMT devices [Fig. 2(b)]. To ensure that the unirradiated devices were of the same quality as compared to the devices irradiated with ^{129}Xe ions, the former devices were exposed to ^{209}Bi ions with higher $(dE/dx)_e$ but with lower fluence. From the corresponding irradiation parameters, we suggest that the degradation of electrical properties is closely related to $(dE/dx)_e$ of the incident ions.

Fig. 3 shows the output characteristics of the devices for different V_{gs} values. The results for the two devices are shown in Fig. 3(a) and (b). It is seen in Fig. 3(b) that I_{ds} increased with the increase in V_{ds} values, achieved a saturation value at V_{ds} = 4 V, and finally adopted a linear trend at V_{ds} = 2 V for the device irradiated with ^{209}Bi ions. The maximum saturation current I_{ds} decreased by almost two orders of magnitude at V_{gs} = −1 V. Moreover, reverse leakage current was detected, and it was found that it reached 3 mA when V_{gs} was set to −4 V and then decreased with the increase in V_{gs} values as shown in Fig. 3(b); this is marked with a red circle. I_{ds} remained nearly constant and was approximately the same for all negative V_{gs} values in the saturation region. Although the saturation current I_{ds} was controlled by V_{gs}, the ability to adjust I_{ds} was found to be weakened in this case. This implies that additional traps were induced under the gate area as a result of the SHI irradiation. Fig. 3(c) and (d) display the variation in I_{ds} for the devices irradiated with ^{129}Xe ions. In the case of V_{gs} = 0 V and drain-source voltage V_{ds} = 10 V, I_{ds} was found to decrease mainly from 290 mA to 100 mA. However, no reverse leakage current was detected in ^{129}Xe ion-irradiated devices (see the inset in Fig. 3(d)). These results confirmed that the degradation in electrical properties of the devices was more significantly induced by irradiation with ^{209}Bi ion than that with ^{129}Xe ions.

3.2. Transmission electron microscopy (TEM) analysis

The cross-sectional imaging of the devices was performed by TEM characterization. Fig. 4 shows the images of the devices irradiated with 1540-MeV ^{209}Bi ions at a fluence of 1.7×10^{11} ions/cm^2. The ion tracks were first visualized in TEM passing through the whole gate and heterogeneous junction thickness as shown in Fig. 4(a). The high-resolution images of the tracks presented in Fig. 4(a) are marked with dotted rectangular areas shown in Fig. 4(b) and (c). It is interesting to note that the bubble-like tracks formed near the AlGaN barrier layer are quasi-continuous with an external diameter of approximately 5.8 nm, and the continuity of the tracks reduced sharply with the increase in depth of the buffer layer. In GaN layer, the tracks were visualized as indicated by the brighter area with a maximum diameter of about 4.3 nm at a depth of 500 nm from the surface of the devices, where some parts in the image seem to be even amorphous. We also observed the tracks through the entire drain layer in the device as shown in Fig. 4(d). It is seen that these tracks are quasi-continuous at a depth of 500 nm in GaN layer as

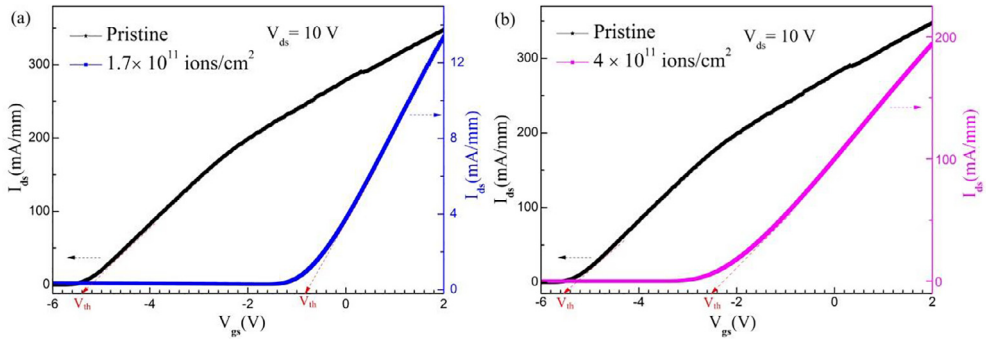

Fig. 2. Transfer characteristic curves of AlGaN/GaN HEMT devices before and after irradiation with (a) 1540-MeV ^{209}Bi ions at a fluence of 1.7 × 10^{11} ions/cm^2 and (b) 2300-MeV ^{129}Xe ions at a fluence of 4 × 10^{11} ions/cm^2. The arrows indicate the coordinates of each curve.

shown in Fig. 4(e).

Fig. 5 shows the images of the devices irradiated with 2300-MeV ^{129}Xe ions at a fluence of 4 × 10^{11} ions/cm^2. It was found that no tracks appeared in the whole section, and the GaN epitaxial layer remained in crystalline form. The selected area electron diffraction (SAED) shown in the inset of Fig. 5(b) does not show any visible amorphous halo; this indicates that the proportion of crystalline phase was sufficiently large. According to SRIM-2013 code calculations, $(dE/dx)_e$ of ^{129}Xe ions just reached its threshold value of 22.8 keV/nm from the literature report [22]; however, no tracks were observed in the devices. On the basis of this analysis, it is speculated that the threshold of $(dE/dx)_e$ for track formation under ^{129}Xe ion irradiation was above 23 keV/nm in GaN materials.

As reported by Sall et al. [23], the tracks introduced in GaN are visible only near the surface after irradiation with 106-MeV ^{238}U ions with $(dE/dx)_e$ of 24 keV/nm. In the study by Kucheyev et al. [24], discontinuous tracks were observed along the ion path in GaN with 200-MeV Au ions at $(dE/dx)_e$ value of 34 keV/nm. In this work, no tracks were observed in the device after irradiation with ^{129}Xe at $(dE/dx)_e$ of 22.9 keV/nm, while the quasi-continuous tracks were first discovered in AlGaN/GaN device induced by ^{209}Bi ions at $(dE/dx)_e$ of 45.9, and part of them even appeared amorphous. It is important to note that SHI irradiation results in a sharp drop in continuity of the tracks with the increase in the depth of GaN layer. An explanation for this trend is based on thermal spike model [25,26]. The transfer of energy loss into the material through electron phonon coupling results in localized melting, and upon rapid quenching, the melt may solidify in amorphous phase along the trajectory of SHIs [27]. Thermal spike model also concludes that only a considerable kinetic energy of the projectile can lead to localized melting along the ion path and creates the tracks [24]. The electronic stopping power was measured by $(dE/dx)_e$ of the SHI. As reported in the literature [22,28], the threshold of $(dE/dx)_e$ for the track formation was found in the range 22.8–28.3 keV/nm in GaN bulk materials, and both of them depend on the ion beam parameters and material characteristics. In addition, it is known that the ions undergo charge state fluctuations along their path that can also lead to the variation in $(dE/dx)_e$. In the case of ^{129}Xe ions, $(dE/dx)_e$ is close to the threshold value. The variations in $(dE/dx)_e$ caused by various reasons eventually lead the $(dE/dx)_e$ to be below the threshold value, and thus, no tracks were observed. In the case of ^{209}Bi ions, at a depth of 500 nm,

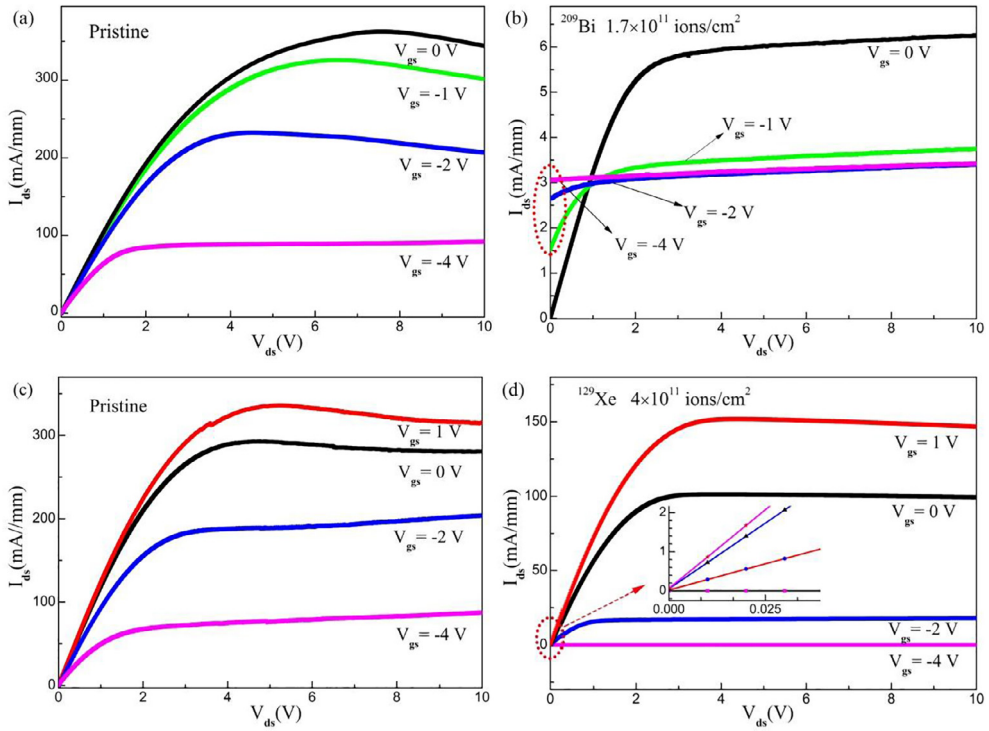

Fig. 3. Output characteristic curves of AlGaN/GaN HEMT devices (a) before and (b) after irradiation with 1540-MeV ^{209}Bi ions, and output characteristic curves of (c) pristine and (d) irradiated devices with 2300-MeV ^{129}Xe ions.

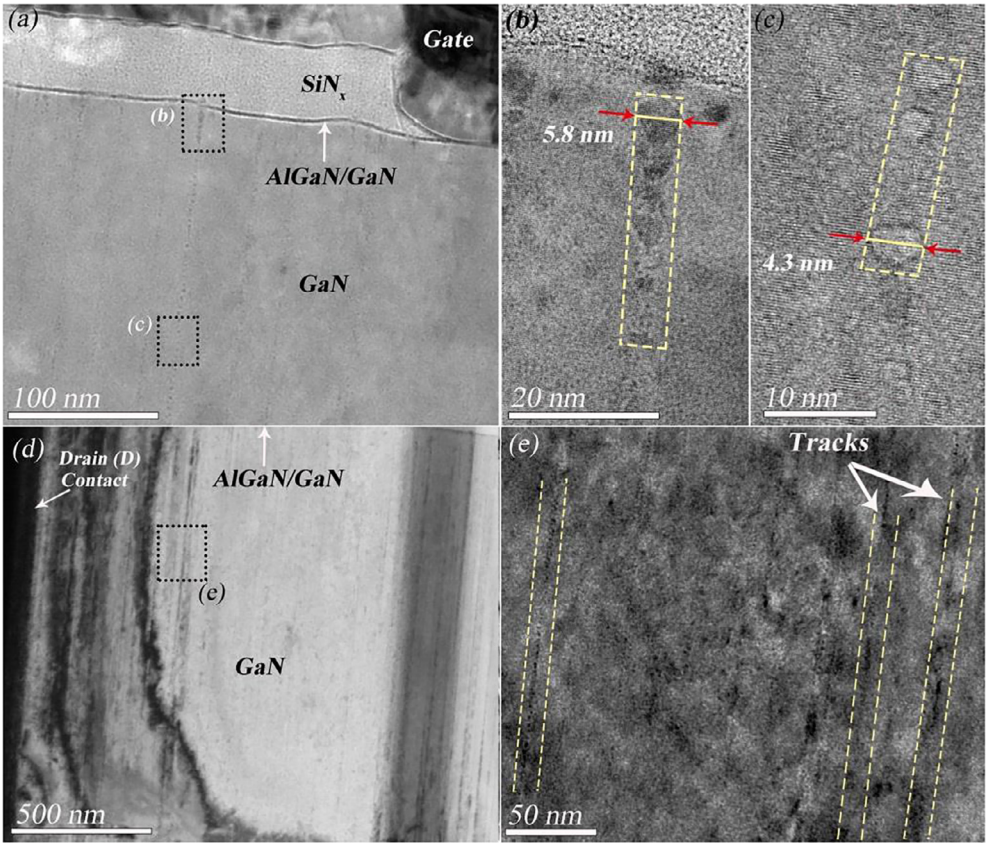

Fig. 4. XTEM images of AlGaN/GaN HEMT device irradiated with 1540-MeV ^{209}Bi ions at a fluence of 1.7×10^{11} ions/cm^2: (a) cross-section of the gate areas; (b) High-resolution image of the tracks in heterogeneous junction areas as marked in figure (a); (c) High-resolution image of the tracks at a depth of about 500 nm as marked in figure (a); (d) Tracks formed in the drain area; (e) Tracks appear at a depth of about 500 nm as marked in figure (d).

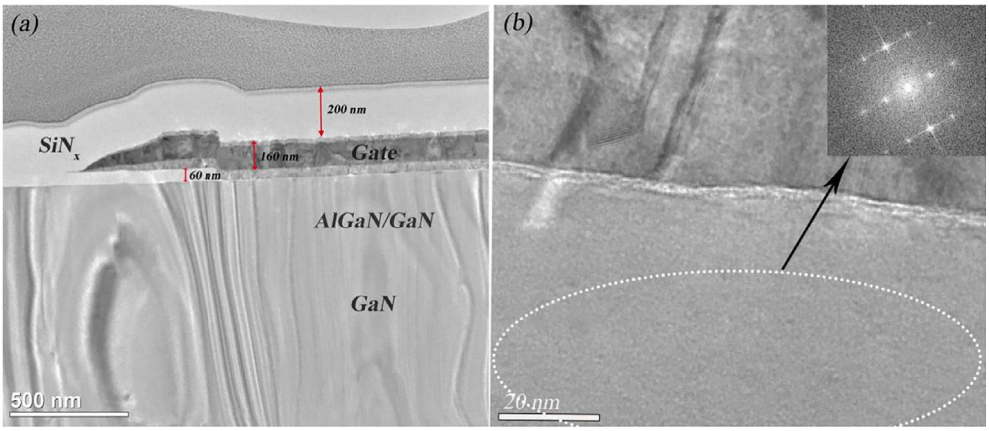

Fig. 5. XTEM images of GaN samples irradiated with 2300-MeV ^{129}Xe ions at a fluence of 4×10^{11} ions/cm^2 (a) represents the source and gate areas; (b) represents high-resolution image of the cross-section under the gate area.

the energy of the incident ions was reduced to 1500 MeV, but the $(dE/dx)_e$ was increased to 46.1 keV/nm. This is too high above the threshold value; therefore, the effects of energy fluctuations can be ignored, and quasi-continuous tracks were observed. As shown in Fig. 5(a), the thickness of the gate electrode was about 160 nm. The SiN_x layer was about 200 nm above the gate area and 60 nm under the tail of the T-type gate. The thickness of the electrode and the passivation layer was too thin to deposit more energy of incident ions. However, the threshold value of the stopping power for direct amorphous track formation is yet to be reached. Therefore, no tracks were observed in the device, but obviously point defects and defect clusters remained there, which can result in a significant deterioration of electrical properties of the devices.

According to previous works [10,14], the degradation of electrical properties of the devices is closely related to the damage of the structure. The incident ions traverse the active areas, thus creating a nearly uniform profile of defects and even producing the tracks throughout the device structure. The track formation also indicates the accumulation of defects or defect clusters in the devices. These defects result in the disorder of the crystal structure and generate lattice stresses in the samples; this result has already been reported in our previous work [29]. Based on simulations, the majority of defects are interstitials, vacancies, and Frenkel pairs, though a few defect clusters likely occur [20]. The decrease in the maximum value of I_{ds} is mainly due to the introduction of deep level defects at the interface of heterogeneous junctions, and the shift in V_{th} is directly proportional to the sheet density [30]. The number of scattering centers from radiation-induced defects near the carrier transport channel including secondary particle ionization and lattice atomic disorder increases the odds of ionized impurity scattering, which leads to a sharp decrease in the

mobility of the carrier in HEMT devices [9,14]. Additionally, the defects introduce the trapped charges near the 2DEG, which results in the decrease in the sheet carrier density [20,31]. These factors are mainly responsible for the degradation of electrical properties of GaN HEMT devices.

4. Conclusions

In conclusion, we studied the degradation of electrical properties and structure damage of AlGaN/GaN HEMT devices after SHI irradiation. An increase in V_{th} and a sharp decrease in I_{ds} were observed in the devices. Quasi-continuous tracks created by ^{209}Bi ions were observed for the first time visually in AlGaN/GaN HEMT devices. Further analyses indicated that the defects and disorders induced by SHI irradiation were responsible for the degradation of the devices, which resulted in the decreased carrier mobility and sheet carrier density of 2DEG. Thus, we propose that the latent tracks play an essential role in the degradation of HEMT devices. Further efforts are required to evaluate the degree of degradation for different $(dE/dx)_e$ values and various fluences of the incident ions.

Acknowledgments

The authors thank the accelerator team of HIRFL of IMP for the technical support and the staff of the School of Physical Science and Technology of Lanzhou University for providing the characterization facilities. This work was financially supported by the National Natural Science Foundation of China (11675233, 11690041, 11375241, 11705246, 11505243, and 11405229). JLD thanks the financial support from the Outstanding Young Scientist Project, Key Research Program of Frontier Sciences, CAS under Grant No. QYZDB-SSW-SLH010.

References

[1] T. Yamasaki, Y. Kittaka, H. Minamide, K. Yamauchi, S. Miwa, S. Goto, M. Nakayama, M. Kohno, N. Yoshida, Proc. Microwave Symposium Digest (MTT) IEEE MTT-S International, 2010, p. 1384.
[2] F. Medjdoub, K. Iniewski (Eds.), Gallium Nitride (GaN) Physics, Devices, and Technology, CRC Press, Boca Raton, 2013.
[3] E.F. Schubert, Light-Emitting Diodes, second ed., Cambridge University Press, Cambridge, 2008.
[4] A.D. Koehler, M.J. Tadjer, T.J. Anderson, P. Chojecki, K.D. Hobart, F.J. Kub, Gallium Nitride and Silicon Carbide Power Technologies 6, 75 (2016) 99–105.
[5] T.J. Anderson, A.D. Koehler, K.D. Hobart, M.J. Tadjer, T.I. Feygelson, J.K. Hite, B.B. Pate, F.J. Kub, C.R. Eddy, IEEE Electron Device Lett. 34 (2013) 1382–1384.
[6] D.J. Meyer, T.I. Feygelson, T.J. Anderson, J.A. Roussos, M.J. Tadjer, B.P. Downey, D.S. Katzer, B.B. Pate, M.G. Ancona, A.D. Koehler, K.D. Hobart, C.R. Eddy, IEEE Electron Device Lett. 35 (2014) 1013–1015.
[7] Y. Sin, J. Bonsall, Z. Lingley, M. Brodie, M. Mason, Gallium Nitride Materials and Devices Xii, 2017, p. 10104.
[8] H. Sasaki, T. Hisaka, K. Kadoiwa, T. Oku, S. Onoda, T. Ohshima, E. Taguchi, H. Yasuda, Microelectron. Reliab. (2017).
[9] B.D. Weaver, P.A. Martin, J.B. Boos, C.D. Cress, IEEE Trans. Nucl. Sci. 59 (2012) 3077–3080.
[10] J.H. Leach, C.Y. Zhu, M. Wu, X. Ni, X. Li, J. Xie, U. Ozgur, H. Morkoc, J. Liberis, E. Sermuksnis, A. Matulionis, H. Cheng, C. Kurdak, Appl. Phys. Lett. 95 (2009).
[11] J.A. del Alamo, J. Joh, Microelectron. Reliab. 49 (2009) 1200–1206.
[12] G. Meneghesso, G. Verzellesi, F. Danesin, F. Rampazzo, F. Zanon, A. Tazzoli, M. Meneghini, E. Zanoni, IEEE Trans. Device Mater. Reliab. 8 (2008) 332–343.
[13] P. Hazdra, S. Popelka, Phys. Status Solidi A 214 (2017).
[14] T.J. Anderson, A.D. Koehler, J.D. Greenlee, B.D. Weaver, M.A. Mastro, J.K. Hite, et al., IEEE Electron Device Lett. 35 (8) (2014) 826.
[15] M.P. Khanal, B. Ozden, K. Kim, S. Uprety, V. Mirkhani, K. Yapabandara, A.C. Ahyi, M. Park, Process. Meas. Phenom. 35 (2017) 03D107.
[16] L. Lv, P.X. Li, X.H. Ma, L.Y. Liu, L. Yang, X.W. Zhou, J.C. Zhang, Y.R. Cao, Z. Bi, T. Jiang, Q. Zhu, Y. Hao, IEEE Trans. Nucl. Sci. 64 (2017) 643–647.
[17] S.O. Kucheyev, J.S. Williams, S.J. Pearton, Mater. Sci. Eng. R 33 (2001) 51–107.
[18] A.Y. Polyakov, S.J. Pearton, P. Frenzer, F. Ren, L. Liu, J. Kim, J. Mater. Chem. C 1 (2013) 877–887.
[19] Y.Z. Yue, Y. Hao, J.C. Zhang, et al., J. Xidian Univ. 35 (1) (2008) 125.
[20] J.F. Ziegler, M.D. Ziegler, J.P. Biersack, Nucl. Instr. Meth. B 268 (2010) 1818–1823.
[21] J. Ziegler, J. Biersack, M. Ziegler, D. Marwick, G. Cuomo, W. Porter, et al., SRIM-2013 Code.
[22] S. Mansouri, P. Marie, C. Dufour, G. Nouet, I. Monnet, H. Lebius, Nucl. Instr. Meth. B 266 (2008) 2814–2818.
[23] M. Sall, I. Monnet, F. Moisy, C. Grygiel, S. Jublot-Leclerc, S. Della-Negra, M. Toulemonde, E. Balanzat, J. Mater. Sci. 50 (2015) 5214–5227.
[24] S.O. Kucheyev, H. Timmers, J. Zou, J.S. Williams, C. Jagadish, G. Li, J. Appl. Phys. 95 (2004) 5360–5365.
[25] O. Herre, W. Wesch, E. Wendler, P.I. Gaiduk, F.F. Komarov, S. Klaumunzer, P. Meier, Phys. Rev. B 58 (1998) 4832–4837.
[26] A. Kamarou, W. Wesch, E. Wendler, A. Undisz, M. Rettenmayr, Phys. Rev. B 73 (2006).
[27] E. Akcoltekin, T. Peters, R. Meyer, A. Duvenbeck, M. Klusmann, I. Monnet, H. Lebius, M. Schleberger, Nat. Nanotechnol. 2 (2007) 290–294.
[28] M. Karlusic, R. Kozubek, H. Lebius, B. Ban-d'Etat, R.A. Wilhelm, M. Buljan, Z. Siketic, F. Scholz, T. Meisch, M. Jaksic, S. Bernstorff, M. Schleberger, B. Santic, J. Phys. D Appl. Phys. 48 (2015).
[29] P.P. Hu, J. Liu, S.X. Zhang, K. Maaz, J. Zeng, H. Guo, P.F. Zhai, J.L. Duan, Y.M. Sun, M.D. Hou, Nucl. Instr. Meth. B 372 (2016) 29–37.
[30] A.P. Karmarkar, B. Jun, D.M. Fleetwood, R.D. Schrimpf, R.A. Weller, B.D. White, L.J. Brillson, U.K. Mishra, IEEE Trans. Nucl. Sci. 51 (2004) 3801–3806.
[31] A.D. Koehler, T.J. Anderson, B.D. Weaver, M.J. Tadjer, K.D. Hobart, F.J. Kub, 2013 1st IEEE Workshop on Wide Bandgap Power Devices and Applications (Wipda), 2013, pp. 112–114.